Impact of stochastic primordial magnetic fields on the scalar contribution to cosmic microwave background anisotropies

Fabio Finelli*
INAF/IASF-BO, Istituto di Astrofisica Spaziale e Fisica Cosmica di Bologna via Gobetti 101, I-40129 Bologna, Italy
INAF/OAB, Osservatorio Astronomico di Bologna, via Ranzani 1, I-40127 Bologna, Italy
INFN, Sezione di Bologna, Via Irnerio 46, I-40126 Bologna, Italy

Francesco Paci+
Dipartimento di Astronomia, Università degli Studi di Bologna, via Ranzani 1, I-40127 Bologna, Italy
INAF/IASF-BO, Istituto di Astrofisica Spaziale e Fisica Cosmica di Bologna via Gobetti 101, I-40129 Bologna, Italy
INFN, Sezione di Bologna, Via Irnerio 46, I-40126 Bologna, Italy

Daniela Paoletti‡
Dipartimento di Fisica, Università degli Studi di Ferrara, via Saragat 1, I-44100 Ferrara, Italy
INAF/IASF-BO, Istituto di Astrofisica Spaziale e Fisica Cosmica di Bologna via Gobetti 101, I-40129 Bologna, Italy
INFN, Sezione di Bologna, via Irnerio 46, I-40126 Bologna, Italy
(Received 14 March 2008; published 9 July 2008)

We study the impact of a stochastic background of primordial magnetic fields on the scalar contribution of cosmic microwave background (CMB) anisotropies and on the matter power spectrum. We give the correct initial conditions for cosmological perturbations and the exact expressions for the energy density and Lorentz force associated to the stochastic background of primordial magnetic fields, given a power-law for their spectra cut at a damping scale. The dependence of the CMB temperature and polarization spectra on the relevant parameters of the primordial magnetic fields is illustrated.

DOI: 10.1103/PhysRevD.78.023510 PACS numbers: 98.80.Cq

I. INTRODUCTION

Large-scale magnetic fields are almost everywhere in the Universe, from galaxies up to those present in galaxy clusters and in the intercluster medium [1]. The dynamo effect provides a mechanism to explain the observed magnetic fields associated to galaxies, whereas those associated to clusters may be generated by gravitational compression. Both these mechanisms require an initial magnetic seed, although with different correlation length.

A possible explanation for this initial seed has driven the interest in primordial magnetic fields in the early universe. Cosmology described by a homogeneous and isotropic expanding metric neither supports a uniform magnetic field nor a gravitational amplification of gauge fields because of conformal invariance; the generation of large-scale magnetic fields has therefore generated a lot of interest. A stochastic background (SB) of primordial magnetic fields (PMF) can provide the initial seeds for the large-scale magnetic fields observed, but can also leave imprints on different observables, as the cosmic microwave background (CMB) pattern of temperature and polarization anisotropies [2,3] and the matter power spectrum.

A SB of PMF is modeled with zero energy and pressure at the homogeneous level in a Robertson-Walker metric. This SB carries perturbations, of any kind, i.e. scalar, vector, and tensor, and it is usually studied in a quasilinear approximation, i.e. its energy momentum tensor (EMT)—quadratic in the magnetic fields amplitude—is considered at the same footing as first order terms in a perturbative series expansion. Vector [4,5] and tensor [4,6,7] metric perturbations sourced by a PMF SB have been the object of several investigations. Beyond the technical simplicity of vector and tensor over scalar, the former are not generated by a perfect fluid and therefore represent a key prediction of a PMF SB. We know, however, that temperature and polarization anisotropies sourced by scalar fluctuations with adiabatic initial conditions are a good fit to the whole set of observations; it is therefore crucial to investigate how a PMF SB can modify these scalar fluctuations. Analytic [8] and numerical [9–11] works in this direction have already been made. However, a detailed analysis which takes into account the Lorentz force on baryons, a careful treatment of initial conditions, and an accurate treatment of the Fourier spectra of the PMF EMT is still lacking. As is clear in the following, our work addresses carefully these issues.

The goal of this paper is to investigate the impact of a SB of PMF on scalar cosmological perturbations and, in particular, on CMB temperature anisotropies and matter power spectrum. Our paper is organized as follows. In Sec. II we review how to add a fully inhomogenous SB of PMF treated in the one-fluid plasma description [2] to

*finelli@iasfbo.inaf.it
+paci@iasfbo.inaf.it
‡paoletti@iasfbo.inaf.it

the Einstein-Boltzmann system of equations. In Secs. III and IV we review the baryons evolution and we give the initial conditions for cosmological perturbations in a form suitable to be plugged in most of the Einstein-Botzmann codes. In Sec. V we give the PMF energy density and Lorentz force power spectra and compare our results with the ones given in the literature. In Secs. VI, VII, and VIII we show the results obtained by our modification of the Einstein-Boltzmann code CAMB [12] for cosmological scalar perturbations, CMB spectrum of temperature and polarization, and matter power spectrum, respectively. In the appendix we show the detailed calculations for the convolution integrals leading to the energy density and Lorentz force, starting from a power-law spectrum sharply cut at a given scale for the PMF.

II. STOCHASTIC MAGNETIC FIELDS AND COSMOLOGICAL SCALAR PERTURBATIONS

We model a SB of PMF as a fully inhomogenous component, considering B^2 at the same level of metric and density fluctuations in a perturbative expansion.[1] Although a SB of PMFs carries no energy at the homogeneous level, it affects scalar cosmological perturbations in three different ways. First, inhomogeneous PMFs carry energy density and pressure and therefore gravitate at the level of perturbations. Second, inhomogeneous PMFs have anisotropic stress—differently from perfect fluids—which adds to the photon and neutrino ones, with the caveat that the photon anisotropic stress is negligible before the decoupling epoch. Last, but not least, inhomogeneous PMFs induce a Lorentz force on baryons, which indirectly affects also photons during the tight-coupling regime.

At linear order PMFs evolve like a stiff source and therefore it is possible to discard all the backreaction of gravity onto the SB of PMF. Before the decoupling epoch the electric conductivity of the primordial plasma is very large, therefore it is possible to consider the infinite conductivity limit, in which the induced electric field is zero. Within the infinite conductivity limit the SB of PMF time evolution simply reduces to: $\mathbf{B}(\mathbf{x}, \tau) = \mathbf{B}(\mathbf{x})/a(\tau)^2$.[2]

The evolution of the metric perturbations in the presence of the PMF is governed by the Einstein equations:

$$G_{\mu\nu} = 8\pi(T_{\mu\nu} + \tau^{\rm PMF}_{\mu\nu}). \tag{1}$$

In the infinite conductivity limit the EMT of PMF:

$$\tau_0^{0\rm PMF} = -\rho_B = -\frac{|\mathbf{B}(\mathbf{x})|^2}{8\pi a^4}, \tag{2}$$

$$\tau_i^{0\rm PMF} = 0, \tag{3}$$

$$\tau_j^{i\rm PMF} = \frac{1}{4\pi a^4}\left(\frac{|\mathbf{B}(\mathbf{x})|^2}{2}\delta^i_j - B_j(\mathbf{x})B^i(\mathbf{x})\right). \tag{4}$$

In the Fourier space[3] the Einstein equations with the contribution of PMF in the synchronous gauge are

$$\begin{aligned} k^2\eta - \frac{1}{2}\mathcal{H}\dot{h} &= 4\pi G a^2(\Sigma_n \rho_n \delta_n + \rho_B), \\ k^2\dot{\eta} &= 4\pi G a^2 \Sigma_n (\rho_n + P_n)\theta_n, \\ \ddot{h} + 2\mathcal{H}\dot{h} - 2k^2\eta &= -8\pi G a^2\left(\Sigma_n c_{sn}^2 \rho_n \delta_n + \frac{\rho_B}{3}\right), \\ \ddot{h} + 6\ddot{\eta} + 2\mathcal{H}(\dot{h} + 6\dot{\eta}) - 2k^2\eta &= -24\pi G a^2 \times [\Sigma_n(\rho_n + P_n)\sigma_n + \sigma_B], \end{aligned} \tag{6}$$

where by n we label the components, i.e. baryons, cold dark matter (CDM), photons, and neutrinos. The PMF EMT conservation— $\nabla_\mu \tau^{\mu\rm PMF}_\nu = 0$—leads to

$$\sigma_B = \frac{\rho_B}{3} + L, \tag{7}$$

where σ_B represents the PMFs anisotropic stress and L the Lorentz force. The energy density of PMF evolves like radiation: $\rho_B(\mathbf{x}, \tau) = \rho_B(\mathbf{x}, \tau_0)/a(\tau)^4$.

III. BARYONS EVOLUTION

The presence of PMFs in a globally neutral plasma induces a Lorentz force on baryons. The general expression for the Lorentz force is [8]:

$$L_i(x, \tau_0) = \frac{1}{4\pi}\left[B_j(\mathbf{x})\nabla_j B_i(\mathbf{x}) - \frac{1}{2}\nabla_i B^2(\mathbf{x})\right], \tag{8}$$

where $\mathbf{L}(x, \tau) = \frac{\mathbf{L}(x,\tau_0)}{a^4}$. We are interested only in the scalar perturbations and the scalar part of the Lorentz force defined as $\nabla^2 L^{(S)} \equiv \nabla_i L_i$ is therefore

$$\nabla^2 L^{(S)} = \frac{1}{4\pi}\left[(\nabla_i B_j(\mathbf{x}))\nabla_j B_i(\mathbf{x}) - \frac{1}{2}\nabla^2 B^2(\mathbf{x})\right]. \tag{9}$$

[1] Note that in such a way we do not take into account the modification of the sound speed of baryons induced by PMFs, pionereed in [13], since it would be technically of second order in the equations of motion. However, since the baryons speed of sound goes rapidly to zero in the matter dominated era, this effect, leading to a shift in the Doppler peaks, may be anyway important.

[2] We choose the standard convention in which at present time t_0, $a(t_0) = 1$.

[3] As Fourier transform and its inverse, we use—in agreement with [14]—:

$$\begin{aligned} Y(\vec{k}, \tau) &= \int \frac{d^3x}{(2\pi)^3} e^{-i\vec{k}\cdot\vec{x}} Y(\vec{x}, \tau), \\ Y(\vec{x}, \tau) &= \int d^3k e^{i\vec{k}\cdot\vec{x}} Y(\vec{k}, \tau), \end{aligned} \tag{5}$$

where Y is a generic function.

In the presence of an electromagnetic source the conservation equations of the baryon component of the primordial fluid becomes

$$\nabla_\mu \delta T^{\mu\nu\,\mathrm{baryons}} \propto F^{\mu\nu} J_\mu, \tag{10}$$

where J_μ is the quadrivector of the density current and $F^{\mu\nu}$ is the Maxwell tensor. The primordial plasma can be considered globally neutral, this leads to $J_0 = 0$ and therefore to the fact that the energy conservation of baryons is not modified by the presence of the Lorentz term. The Euler equation for baryons is instead affected by the Lorentz force and the scalar part is therefore [2]:

$$\dot{\theta}_b = -\mathcal{H}\theta_b + k^2 c_{sb}^2 \delta_b - k^2 \frac{L}{\rho_b}. \tag{11}$$

Now we study how the tight-coupling regime is modified by the presence of a SB of PMF [15]. The Euler equation for photons during the tight-coupling regime is

$$\dot{\theta}_\gamma = k^2\left(\frac{\delta_\gamma}{4} - \sigma_\gamma\right) + a n_e \sigma_T(\theta_b - \theta_\gamma). \tag{12}$$

Combining the photons and baryons equations gives

$$\dot{\theta}_b = \frac{-\mathcal{H}\theta_b + c_s^2 k^2 \delta_b + k^2 R(\frac{\delta_\gamma}{4} - \sigma_\gamma) + R(\dot{\theta}_\gamma - \dot{\theta}_b) - \frac{k^2 L}{\rho_b}}{(1+R)},$$

with

$$\dot{\theta}_b - \dot{\theta}_\gamma = \frac{2R}{(1+R)}\mathcal{H}(\theta_b - \theta_\gamma) + \frac{\tau}{(1+R)}\left(-\frac{\ddot{a}}{a}\theta_b + -\frac{\mathcal{H}k^2}{2}\delta_\gamma + k^2\left(c_s^2\dot{\delta}_b - \frac{\dot{\delta}_\gamma}{4}\right) + \mathcal{H}k^2\frac{L}{\rho_b}\right).$$

The photon Euler equation in the tight-coupling regime instead is

$$\dot{\theta}_\gamma = -R^{-1}\left(\dot{\theta}_b + \mathcal{H}\theta_b - c_s^2 k^2 \delta_b + k^2 \frac{L}{\rho_b}\right) + k^2\left(\frac{\delta_\gamma}{4} - \sigma_\gamma\right). \tag{13}$$

We note that there is a term depending on the Lorentz force which disappears when the tight-coupling ends, leaving the normal Euler equation for the photon velocity.

IV. INITIAL CONDITIONS

Our study of a SB of PMF requires the initial conditions for scalar cosmological perturbations deep in the radiation era (see [2] for the results in the longitudinal gauge). The magnetized adiabatic mode initial conditions in the synchronous gauge are given by [16]

$$\begin{aligned}
&h = C_1(k\tau)^2, \qquad \eta = 2C_1 - \frac{5+4R_\nu}{6(15+4R_\nu)}C_1(k\tau)^2 - \left[\frac{\Omega_B(1-R_\nu)}{6(15+4R_\nu)} + \frac{L_B}{2(15+4R_\nu)}\right](k\tau)^2,\\
&\delta_\gamma = -\Omega_B - \frac{2}{3}C_1(k\tau)^2 + \left[\frac{\Omega_B}{6} + \frac{L_B}{2(1-R_\nu)}\right](k\tau)^2, \qquad \delta_\nu = -\Omega_B - \frac{2}{3}C_1(k\tau)^2 - \left[\frac{\Omega_B(1-R_\nu)}{6R_\nu}\frac{L_B}{2R_\nu}\right](k\tau)^2,\\
&\delta_b = -\frac{3}{4}\Omega_B - \frac{C_1}{2}(k\tau)^2 + \left[\frac{\Omega_B}{8} + \frac{3L_B}{8(1-R_\nu)}\right](k\tau)^2, \qquad \delta_c = -\frac{C_1}{2}(k\tau)^2,\\
&\theta_\gamma = -\frac{C_1}{18}k^4\tau^3 + \left[-\frac{\Omega_B}{4} - \frac{3}{4}\frac{L_B}{(1-R_\nu)}\right]k^2\tau + k\left[\frac{\Omega_B}{72} + \frac{L_B}{24(1-R_\nu)}\right](k\tau)^3, \qquad \theta_b = \theta_\gamma, \qquad \theta_c = 0,\\
&\theta_\nu = -\frac{(23+4R_\nu)}{18(15+4R_\nu)}C_1 k^4\tau^3 + \left[\frac{\Omega_B(1-R_\nu)}{4R_\nu} + \frac{3}{4}\frac{L_B}{R_\nu}\right]k^2\tau - \left[\frac{(1-R_\nu)(27+4R_\nu)\Omega_B}{72R_\nu(15+4R_\nu)} + \frac{(27+4R_\nu)L_B}{24R_\nu(15+4R_\nu)}\right]k^4\tau^3,\\
&\sigma_\nu = \frac{4C_1}{3(15+4R_\nu)}(k\tau)^2 - \frac{\Omega_B}{4R_\nu} - \frac{3}{4}\frac{L_B}{R_\nu} + \left[\frac{(1-R_\nu)}{R_\nu(15+4R_\nu)}\frac{\Omega_B}{2} + \frac{3}{2}\frac{L_B}{R_\nu(15+4R_\nu)}\right](k\tau)^2,
\end{aligned} \tag{14}$$

where $R_\nu = \rho_\nu/(\rho_\nu + \rho_\gamma)$ and C_1 is the constant which characterizes the regular growing adiabatic mode as given in [14]. We have checked that the result reported in [11] and ours [16] agree.

Note how the presence of a SB of PMFs induces a new independent mode in matter and metric perturbations, i.e. the fully magnetic mode. This new independent mode is the particular solution of the inhomogeneous system of the Einstein-Botzmann differential equations: the SB of PMF treated as a stiff source acts indeed as a force term in the system of linear differential equations. Whereas the sum of the fully magnetic mode with the curvature one can be with any correlation as for an isocurvature mode, the nature of the fully magnetic mode—and therefore its effect—is different: the isocurvature modes are solutions of the homogeneous system (in which all the species have both

background and perturbations), whereas the fully magnetic one is the solution of the inhomogeneous system sourced by a fully inhomogeneous component.

It is interesting to note how the magnetic contribution drops from the metric perturbation at leading order, although it is larger than the adiabatic solution for photons, neutrinos, and baryons. This is due to a compensation which nullifies the sum of the leading contributions (in the long-wavelength expansion) in the single species energy densities and therefore in the metric perturbations. A similar compensation exists for a network of topological defects, which does not carry a background EMT as the PMF SB studied here.[4]

V. MAGNETIC FIELD POWER SPECTRA

Power spectra for the amplitude and the EMT of SB of PMF have been the subject of several investigation [4,6,8,9]. We shall work in the Fourier space according to Eq. (5). We shall consider PMFs with a power-law power spectrum, which therefore are characterized by two parameters: an amplitude A and a spectral index n_B. PMFs are suppressed by radiation viscosity on small scales: we approximate this damping by introducing an ultraviolet cutoff in the power spectrum at the (damping) scale k_D.

The two-point correlation function for a statistically homogeneous and isotropic field is

$$\langle \vec{B}_i^*(\vec{k})\vec{B}_j(\vec{k}')\rangle = \delta^3(\vec{k}-\vec{k}')\Big[(\delta_{ij}-\hat{k}_i\hat{k}_j)\frac{P_B(k)}{2} + \epsilon_{ijl}\frac{k_l}{k}P_H(k)\Big], \tag{15}$$

where ϵ_{ijl} is the totally antisymmetric tensor, P_B and P_H are the nonhelical and helical part of the spectrum for the **B** amplitude, respectively. Scalar cosmological perturbations only couple to the nonhelical part of the spectrum and we shall therefore consider only P_B in the following.

A. Magnetic energy density

As is clear from Eqs. (1)–(3), the EMT for PMF is quadratic in the field amplitude. The PMF energy density spectrum is [9]:

$$|\rho_B(k)|^2 = \frac{1}{128\pi^2 a^8}\int d^3p P_B(\vec{p})P_B(|\vec{k}-\vec{p}|)(1+\mu^2), \tag{16}$$

where $\mu = \frac{\vec{p}(\vec{k}-\vec{p})}{p|\vec{k}-\vec{p}|} = \frac{k\cos\theta - p}{\sqrt{(k^2+p^2-2kp\cos\theta)}}$. As for the two-point function in the coincidence limit, $|\rho_B(k)|^2$ is infrared finite for $n_B > -3$ and needs a prescription in the ultraviolet. Since the spectrum of the components of PMF EMT are relevant for the final impact on cosmological perturbations and CMB anisotropies, it is better to address these points carefully.

The usual choice in the literature is to modify the scalar part two-point function of Eq. (15) for zero helicity as [8]

$$\langle \vec{B}_i^*(\vec{k})\vec{B}_j(\vec{k}')\rangle = \begin{cases} \delta^3(\vec{k}-\vec{k}')(\delta_{ij}-\hat{k}_i\hat{k}_j)\frac{P_B(k)}{2} & \text{for } k < k_D \\ 0 & \text{for } k > k_D \end{cases},$$

with

$$P_B(k) = A\left(\frac{k}{k_*}\right)^{n_B}, \tag{17}$$

where k_* is a reference scale. With such a choice the two-point function in the coincident limit (the mean square of the magnetic field) is

$$\langle B^2(x)\rangle = \int_{k<k_D} d^3k P_B(k) = \frac{4\pi A}{n_B+3}\frac{k_D^{n_B+3}}{k_*^{n_B}}. \tag{18}$$

It is also usual in the literature to give the amplitude of B at a given smearing scale k_S by imposing a Gaussian filter:

$$\langle B^2(x)\rangle_{k_S} = \int d^3k P_B(k)e^{-k^2/k_S^2} = 2\pi A\frac{k_S^{n_B+3}}{k_*^{n_B}}\Gamma\left(\frac{n_B+3}{2}\right). \tag{19}$$

By smearing the magnetic power spectrum and integrating for $k < k_D$, one gets

$$\langle B^2(x)\rangle_{k_S}^{\rm cut} = \int_{k<k_D} d^3k P_B(k)e^{-k^2/k_S^2} = 2\pi A\frac{k_D^{n_B+3}}{k_*^{n_B}}\left[\Gamma\left(\frac{n_B+3}{2}\right) - \Gamma\left(\frac{n_B+3}{2},\frac{k_D^2}{k_S^2}\right)\right], \tag{20}$$

where the incomplete Gamma function $\Gamma(\ldots,\ldots)$ [17] has been introduced. Note how $n_B > -3$ in order to prevent infrared divergencies either in the mean square field or the amplitude of the field smeared at a given scale. In the following by $\langle B^2\rangle$ we mean the value given by Eq. (18). Figure 1 shows how $\langle B^2(x)\rangle_{k_S}$ may be much larger than $\langle B^2\rangle$ for $n_B > 0$.

The exact result for the Fourier convolution leading to the magnetic energy density Fourier square amplitude is one of the new main results of this paper. The convolution involves a double integral, one in the angle between $\boldsymbol{k}$ and $\boldsymbol{p}$ and one in the modulus of $\boldsymbol{p}$. The angular integral, often omitted in the literature, is responsible for a nonvanishing $|\rho_B(k)|^2$ only for $k < 2k_D$. The detailed calculations and the results for the energy density convolutions are given in Appendix A for several values of n_B. The generic behavior for $k \ll k_D$ and $n_B > -3/2$ is white noise with amplitude

$$|\rho_B(k)|^2 \simeq \frac{A^2k_D^{2n+3}}{16\pi k_*^{2n}(3+2n_B)} \tag{21}$$

and then goes to zero for $k = 2k_D$, which is a result

[4]Note, however, that a network of topological defects does not scale with radiation and interacts only gravitationally with the rest of matter, i.e. a Lorentz term is absent.

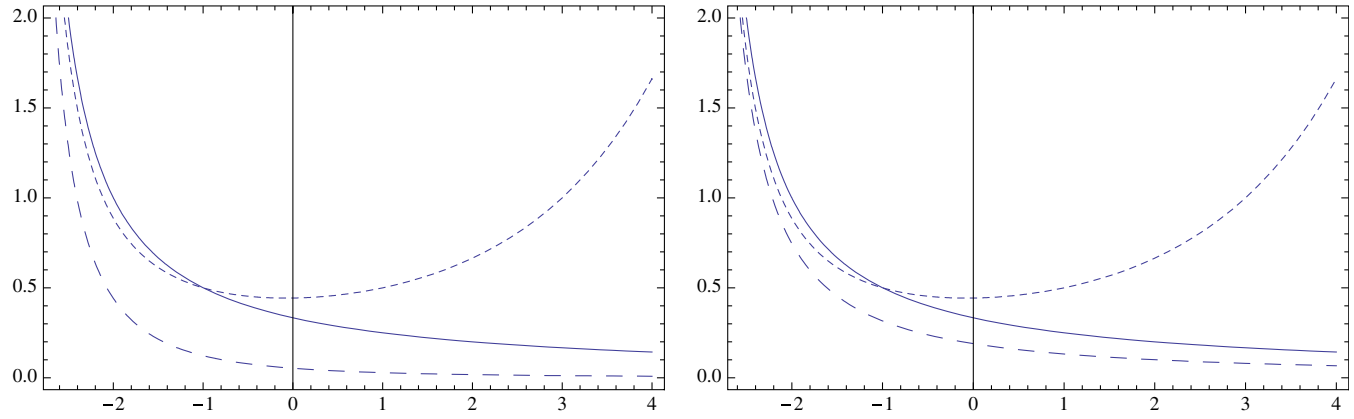

FIG. 1 (color online). Plots of the different ways of computing the magnetic power spectra (in units of $4\pi A k_D^{n_B+3}/k_*^{n_B}$) versus n_B for $k_S = k_D/2$ (left) and $k_S = k_D$ (right). $\langle B^2\rangle$, $\langle B^2\rangle_{k_S}$, $\langle B^2\rangle_{\mathrm{cut},k_S}$ are represented by solid, dotted, and dashed lines, respectively.

obtained by performing correctly the integral. The pole for $n_B = -3/2$ in Eq. (21) is replaced by a logarithmic divergence in k in the exact result; for $n_B < -3/2$ the spectrum is no more white noise for $k \ll k_D$. Figure 2 shows the dependence of $k^3|\rho_B(k)|^2$ on n_B at fixed $\langle B^2\rangle$.

Our result is different from the one reported in the literature [8], which is

$$|\rho_B(k)|^2_{KR} = \frac{3A^2 k_D^{2n_B+3}}{64\pi k_*^{2n_B}(3+2n_B)}\left[1 + \frac{n_B}{n_B+3}\left(\frac{k}{k_D}\right)^{2n_B+3}\right], \tag{22}$$

and is not limited in k. In Fig. 3 we show the difference between the literature result [8] and our result for $n_B = 2, -3/2$. For numerical calculations of the PMF EMT Fourier convolution integrals, see [18,19].

B. Lorentz force

As is clear from previous sections, we also need the Lorentz force

$$|L(k)|^2 = \frac{1}{128\pi^2 a^8}\int d^3p P_B(p) P_B(|\mathbf{k}-\mathbf{p}|)[1+\mu^2 + 4\gamma\beta(\gamma\beta-\mu)], \tag{23}$$

and the magnetic anisotropic stress

$$|\sigma_B(k)|^2 = \frac{1}{288\pi^2 a^8}\int d^3p P_B(p) P_B(|\mathbf{k}-\mathbf{p}|)[9(1-\gamma^2) \times (1-\beta^2) - 6(1+\gamma\mu\beta-\gamma^2-\beta^2) \times (1+\mu^2)], \tag{24}$$

where $\gamma = \hat{k}\cdot\hat{p}$, $\beta = \vec{k}\cdot(\vec{k}-\vec{p})/(k|\vec{k}-\vec{p}|)$ and $\mu = \vec{p}\cdot(\vec{k}-\vec{p})/(p|\vec{k}-\vec{p}|)$.

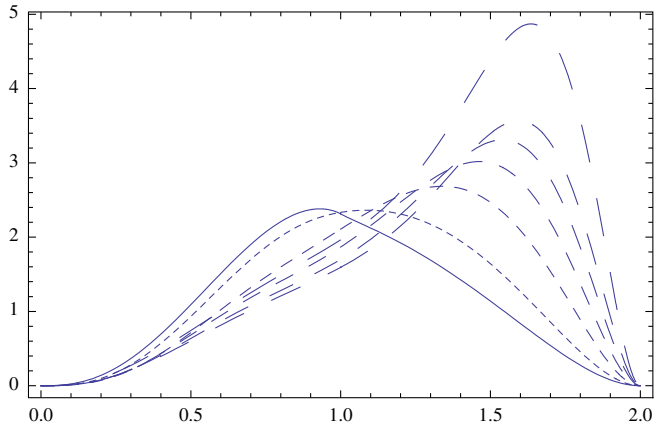

FIG. 2 (color online). Plot of magnetic energy density power spectrum $k^3|\rho_B(k)|^2$ in units of $\langle B^2\rangle^2/(1024\pi^3)$ versus k/k_D for different n_B for fixed $\langle B^2\rangle$. The different lines are for $n_B = -3/2, -1, 0, 1, 2, 3, 4$ ranging from the solid to the longest dashed.

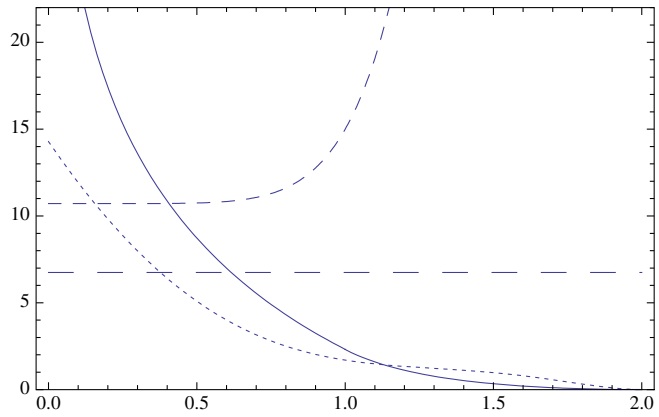

FIG. 3 (color online). Comparison of magnetic energy density convolution $k_D^3|\rho_B(k)|^2$ obtained in this paper (dotted, solid lines) in units of $\langle B^2\rangle^2/(1024\pi^3)$ and the one in Eq. (22) (dashed, long-dashed lines) versus k/k_D for $n_B = 2, -3/2$ with fixed $\langle B^2\rangle$.

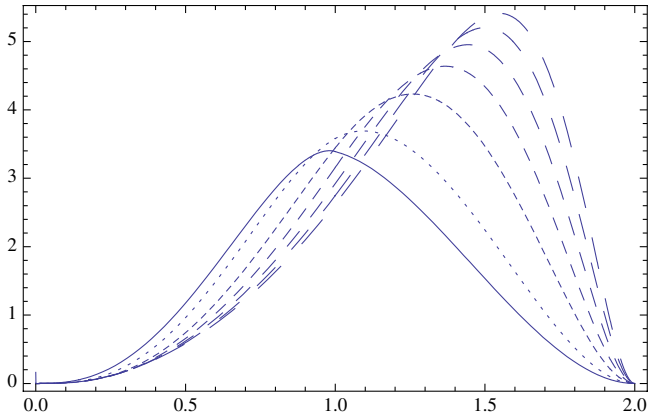

FIG. 4 (color online). Plot of the Lorentz force power spectrum $k^3|L(k)|^2$ in units of $\langle B^2\rangle^2/(1024\pi^3)$ versus k/k_D for different n_B for fixed $\langle B^2\rangle$. The different lines are for $n_B = -3/2,\ -1,\ 0,\ 1,\ 2,\ 3,\ 4$ ranging from the solid to the longest dashed.

We decide to compute the spectrum of the Lorentz force and obtain the anisotropic stress by Eq. (7). The exact computation for the Lorentz force power spectrum is given in Appendix B for several values of n_B. A term $-\rho_B$ can be easily identified in Eq. (9); since we know from the exact computation that the integral of $P_B(p)P_B(|\mathbf{k}-\mathbf{p}|)\times(1+\mu^2)$ is larger than the remaining piece in Eq. (23) we chose the signs for $\rho_B(k)$ and $L(k)$ as opposite.

Figure 4 shows the dependence of $k^3|L(k)|^2$ on n_B at fixed $\langle B^2\rangle$. Figure 5 compares the approximation $L(k) \simeq -\rho_B(k)$ suggested in Ref. [8] with the exact calculation. As can be checked in Appendix B, our exact calculations for the values of n_B studied here show that

$$|L(k)|^2 \simeq \tfrac{11}{15}|\rho_B(k)|^2 \quad \text{for } k \ll k_D. \tag{25}$$

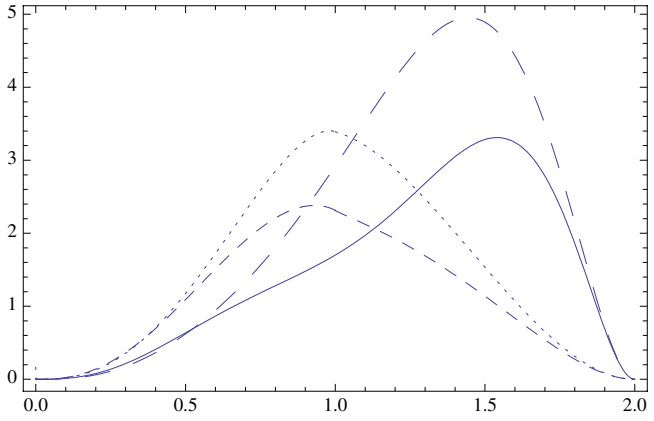

FIG. 5 (color online). Comparison of the magnetic energy density and Lorentz force power spectra versus k/k_D for fixed $\langle B^2\rangle$. The solid (medium dashed) and long-dashed (short-dashed) lines are, respectively, for $k^3|\rho_B(k)|^2$ and $k^3|L(k)|^2$ for $n_B = 2$ ($n_B = -3/2$).

VI. RESULTS FOR COSMOLOGICAL PERTURBATIONS

In order to study the effects of a SB of PMFs on CMB anisotropies and matter power spectrum we modified the CAMB Einstein-Boltzmann code [12] (June 2006 version) by introducing the PMF contribution in the Einstein equations, in the evolution equation for baryons and initial conditions, following Eqs. (6), (11), and (14).

We note that implementing the baryons evolution as from Eq. (11), the MHD approximation in a globally neutral plasma is used up to the present time: this makes the Lorentz term nonvanishing up to the present time. Although the term L/ρ_b in Eq. (11) decreases with time, its effect on the baryon velocity is crucial. At late time—deep in the matter era when the baryons sound speed is effectively zero—baryons velocity can be approximated as

$$\theta_b^{\rm late} \simeq -k^2\left(\frac{La}{\rho_b}\right)\frac{\tau}{a}. \tag{26}$$

Our modified Einstein-Boltzmann code reproduces correctly this asymptotic regime for different wavelengths, as can be seen by Fig. 6. The corresponding effects on the density contrasts for the same wavelengths are shown in Fig. 7. In Fig. 8 the effects due to the pure magnetic mode and due to the correlation with the adiabatic mode are shown. Figure 9 displays the importance of the Lorentz term compared to the purely gravitational effect in the PMF contribution.

VII. RESULTS FOR CMB TEMPERATURE AND POLARIZATION POWER SPECTRA

In this section we show the results on the CMB temperature and polarization pattern obtained by our modifications of the CAMB code. Figure 10 shows the various contributions to the total CMB temperature and polarization angular power spectra from the pure magnetic mode and its correlation with the adiabatic mode. Figure 11 shows the dependence of the total temperature power spectrum on the spectral index n_B. Note that the Lorentz force of a fully correlated magnetic mode decreases the density contrasts. As a consequence the CMB angular power spectrum decreases in an intermediate range of multipoles, as shown in Fig. 12.

VIII. RESULTS FOR THE MATTER POWER SPECTRA

In Fig. 13 we present the results for the linear CDM power spectrum evaluated at present time in the presence of SB of PMF. By analyzing Fourier spectra we have checked that the adiabatic results are recovered for $k > 2k_D$. We compare the results obtained by neglecting or by taking into account the Lorentz term. By considering the equations evolved and the previous figures, it is clear how the Lorentz term treated as in Eq. (11) is a leading con-

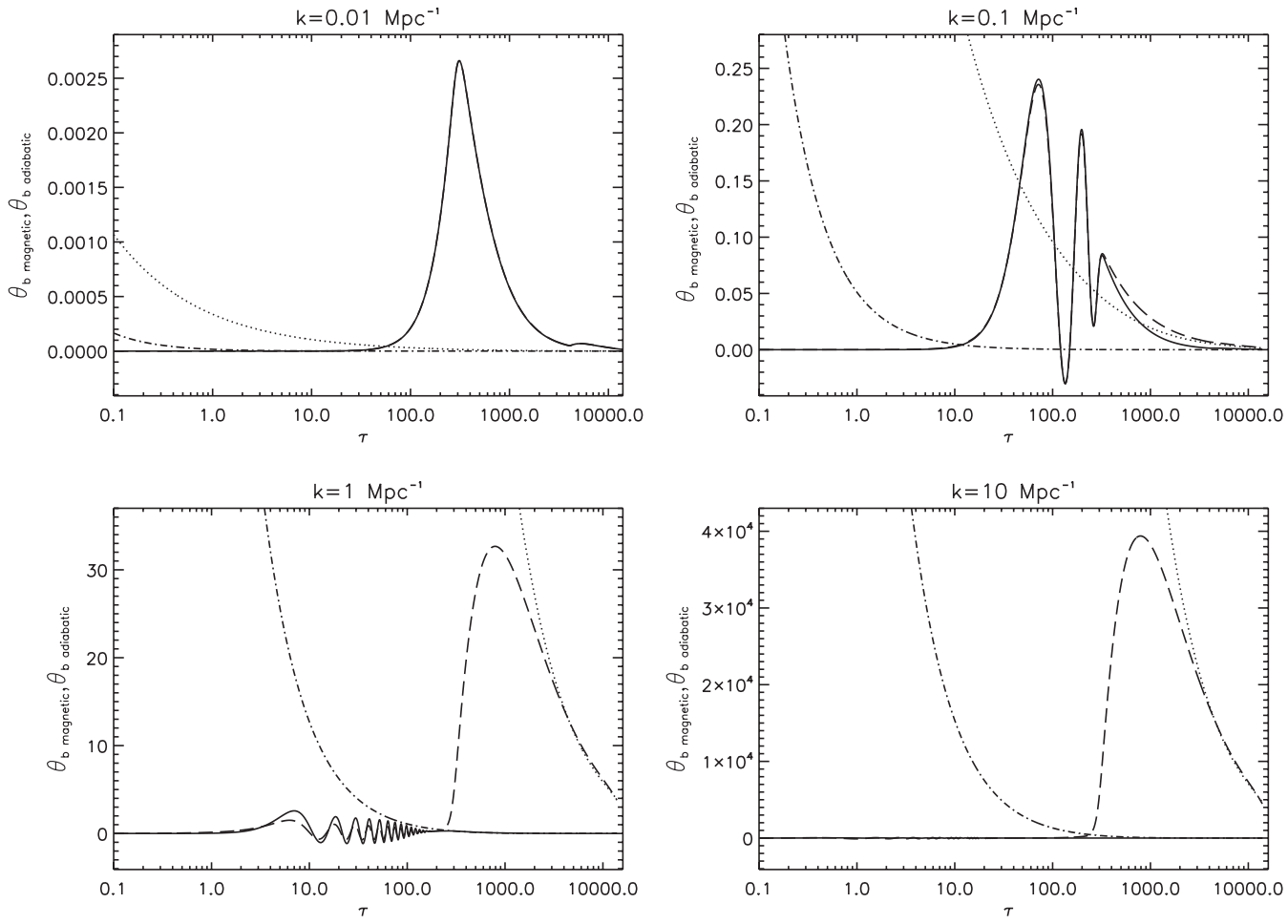

FIG. 6. Evolution of baryons velocity for 4 different wave numbers with (dashed line) and without (solid line) PMF. k^2L/ρ_b (dot-dashed line) and the solution $\theta_b^{\rm late}$ (dotted line) are also plotted: note how the numerics agree with $\theta_b^{\rm late}$ at late times. The cosmological parameters of the flat ΛCDM model are $\Omega_b h^2 = 0.022$, $\Omega_c h^2 = 0.123$, $\tau = 0.04$, $n_s = 1$, $H_0 = 72\ \mathrm{kms}^{-1}\,\mathrm{Mpc}^{-1}$.

tribution for baryons which gives rise to a long-time effect as show in Fig. 6. Through gravity CDM is affected as shown in Figs. 7–9 and therefore a large feature is present in the linear CDM matter PS.

IX. CONCLUSIONS

We have investigated the impact of a SB of PMF on scalar cosmological perturbations and its impact on CMB anisotropies and matter power spectrum. The effects on the CMB angular power spectrum is one of the distinctive features of stochastic PMF together with non-Gaussianities [18] and Faraday rotation [20]: future missions as PLANCK [21] will greatly improve the present constraints [10,22].

We have analyzed the SB of PMF in the one-fluid MHD approximation [2] as a source for cosmological perturbations and we have inserted such modifications in the CAMB code [12]. Our numerical code improves previous studies [10,11] for the treatment of initial conditions and exact convolutions for the PMF EMT. Note that the present constraints [10,22] used neither the correct initial conditions nor the correct convolutions for the PMF energy density and Lorentz force power spectra. Reference [11] uses the correct initial conditions, but a power spectrum for the PMF energy-density with a spectral index which is twice the one for the power spectrum of the magnetic field. We have shown extensively in Sec. VI and Appendix A and B that this is not the case.

We have also shown how the Lorentz term for baryons in the one-fluid plasma description [2] may lead to a long-time effect which we have described analytically in Eq. (26). This last point deserves further investigation.

ACKNOWLEDGMENTS

We are grateful to Chiara Caprini, Ruth Durrer, and Jose Alberto Rubino-Martin for conversations and discussions on magnetic fields. This work has been done in the framework of the Planck LFI activities and is partially supported

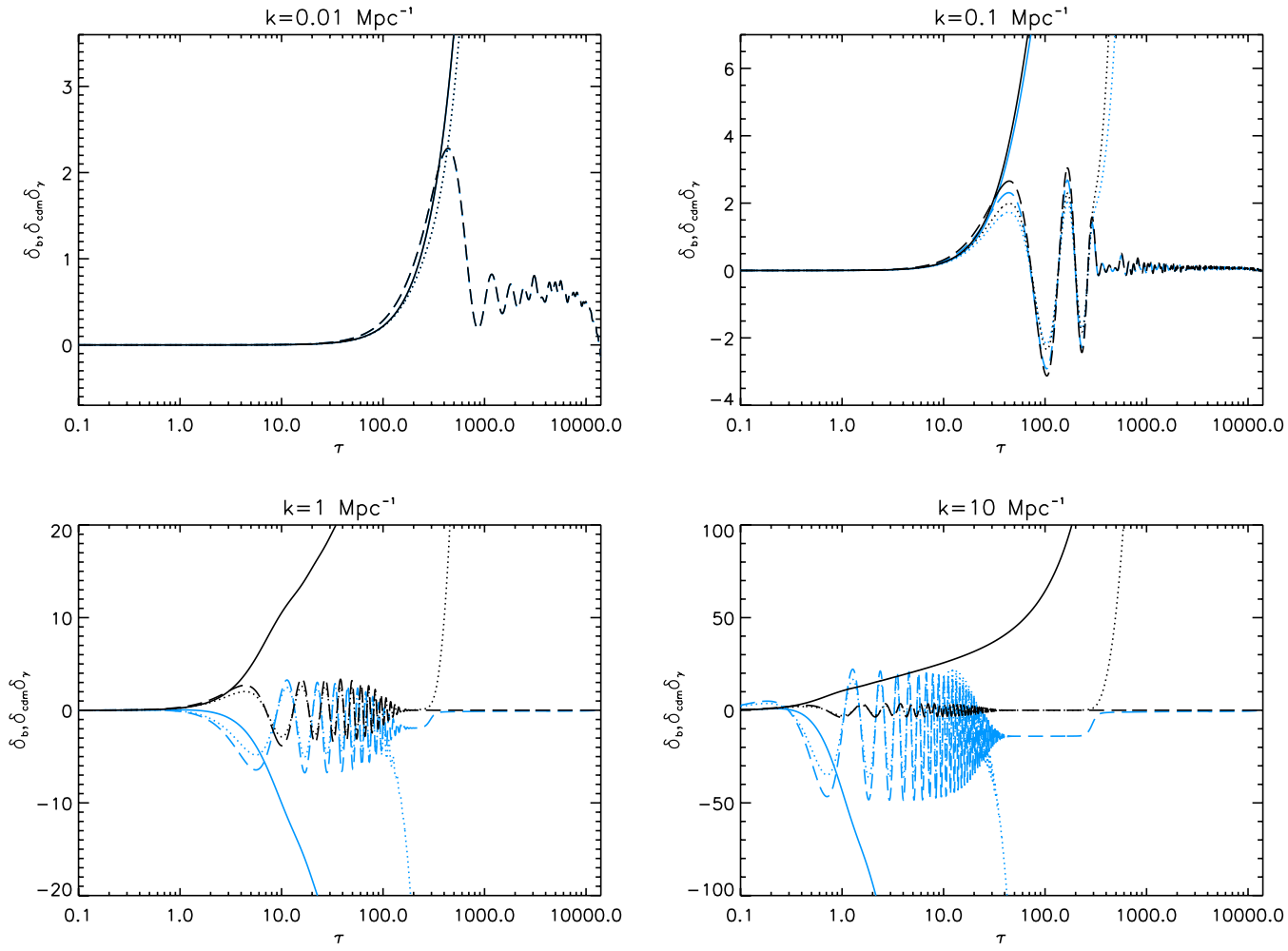

FIG. 7 (color online). Evolution of baryons (dotted line), CDM (solid line), and photons (dashed line) density contrast for 4 different wave numbers with fully correlated (blue, lighter line) and without (black, darker line) PMF. The cosmological parameters are the same as Fig. 6.

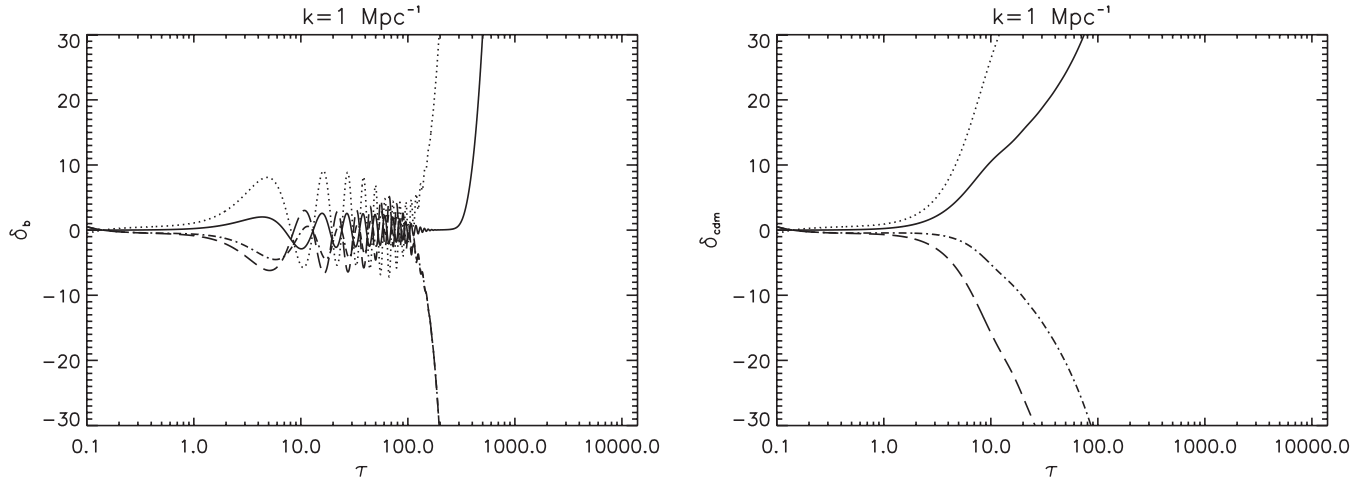

FIG. 8. Time evolution of baryons (left) and CDM (right) density contrasts with vanishing PMF (solid line), fully correlated (dashed line), fully anticorrelated (dotted line), and purely magnetic initial conditions (dot-dashed line). The other cosmological parameters are the same as Fig. 6.

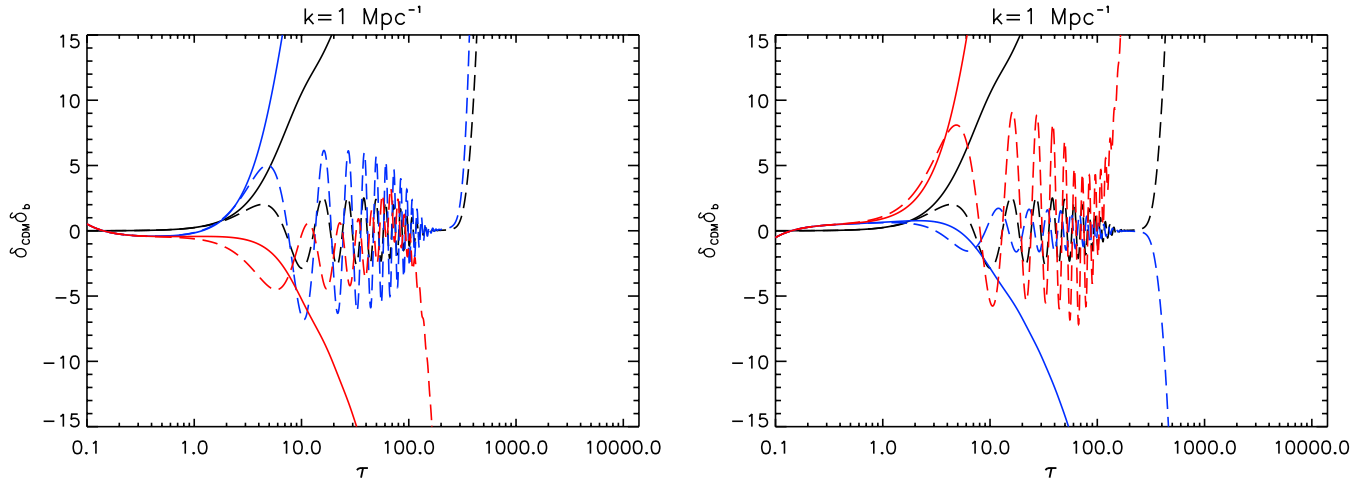

FIG. 9 (color online). Time evolution of baryons (dashed line) and CDM (solid line) density contrasts for purely adiabatic with vanishing PMF (black, darker line), fully correlated (left panel) and anticorrelated (right panel) PMF with vanishing (blue, intermediate line) and nonvanishing (red, lighter line) Lorentz force for $k = 1\ \mathrm{Mpc}^{-1}$. These figures show clearly that the Lorentz force and the gravitational contribution are of opposite sign, and the Lorentz term is more important. The cosmological parameters are the same as Fig. 6.

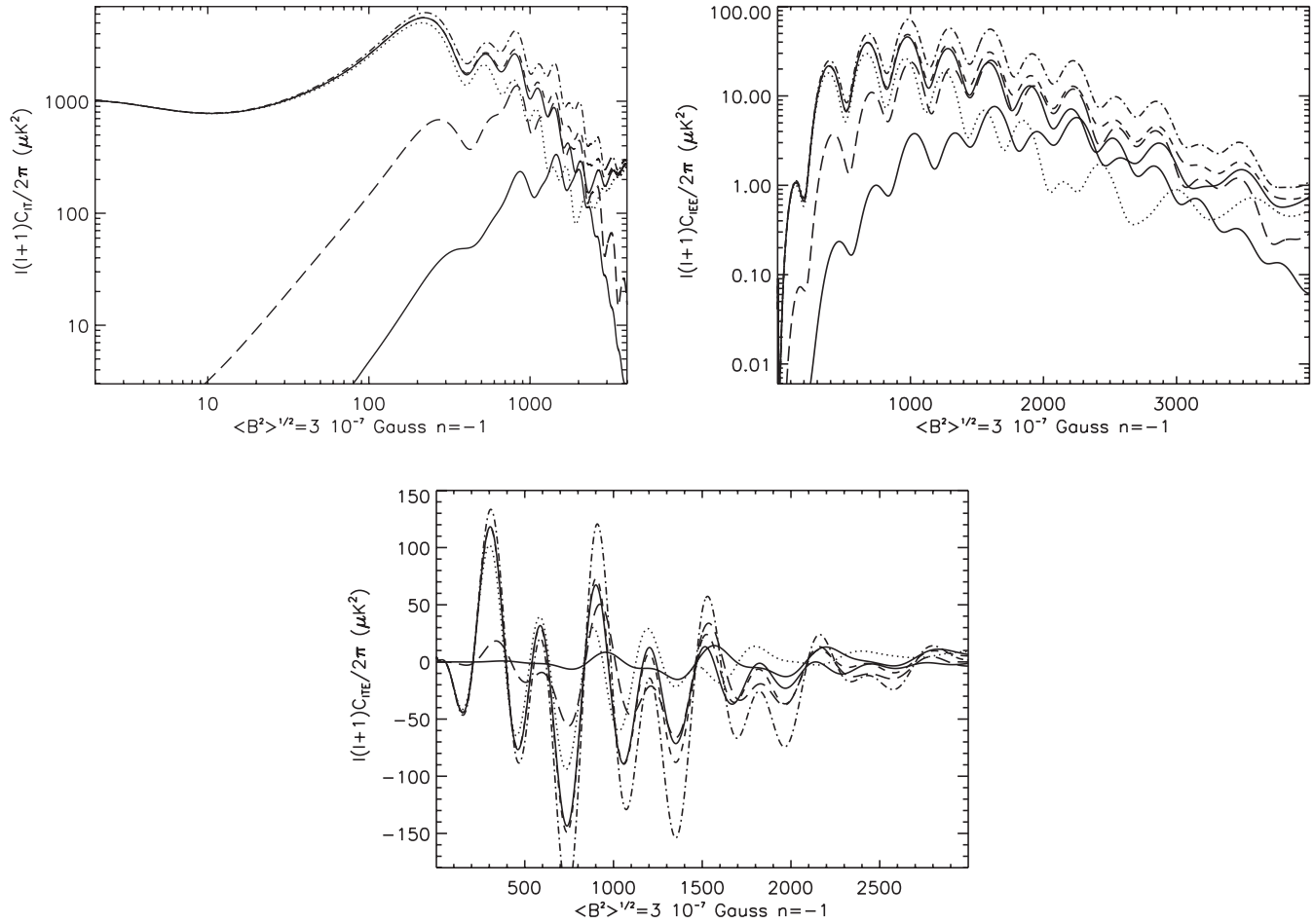

FIG. 10. CMB temperature angular power spectra obtained with $\sqrt{\langle B^2 \rangle} = 3 \times 10^{-7}$ Gauss, $n_B = -1$, $k_D = \pi$ in comparison with the adiabatic spectrum with vanishing PMF (solid line): TT, EE, TE are displayed in the top left, top right, bottom panel, respectively. The purely magnetic, correlation, fully correlated, fully anticorrelated, and uncorrelated spectra are represented as triple dotted-dashed, dashed, dotted, dot-dashed, and long-dashed lines, respectively. The other cosmological parameters are the same as Fig. 6.

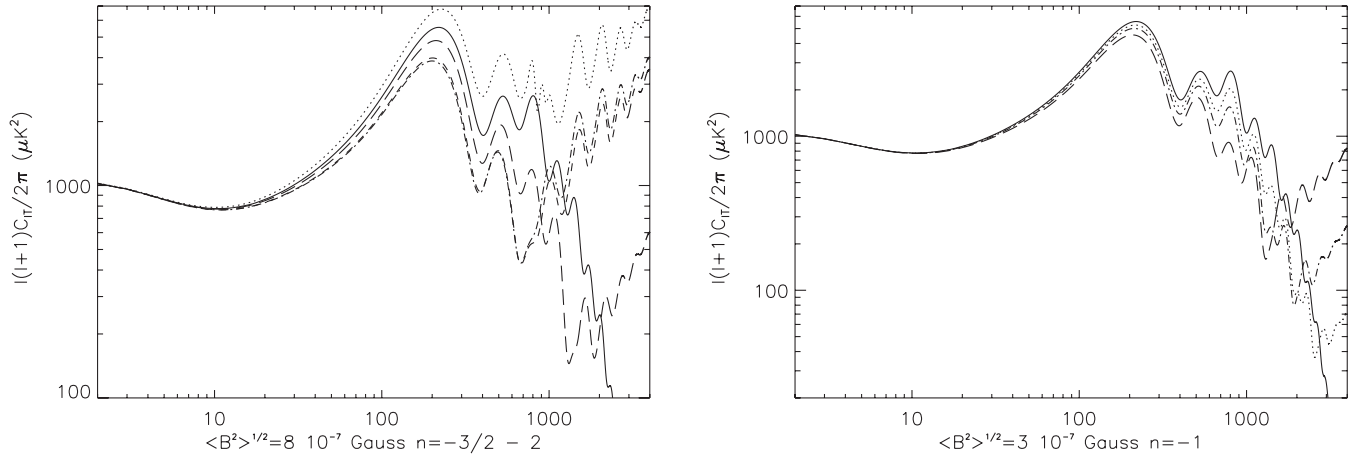

FIG. 11. In the left panel variation of the CMB temperature angular power spectrum with n_B in comparison to the case with vanishing PMF (solid line). In the left figure $\sqrt{\langle B^2\rangle} = 8 \times 10^{-7}$ Gauss, $k_D = 2\pi$ and fully correlated initial conditions are considered. The spectral indexes plotted are $n_B = -3/2,\ -1,\ 1,\ 2$ (dotted, dot-dashed, dashed, and long-dashed lines, respectively). In the right panel, variation of the CMB angular power spectrum with k_D in comparison to the case with vanishing PMF (solid line). In the right figure $\sqrt{\langle B^2\rangle} = 3 \times 10^{-7}$ Gauss, $n_B = -1$, and $k_D = 2\pi,\ \pi,\ \pi/2$ (dotted, dot-dashed, and dashed, respectively). In both panels the initial conditions are fully correlated and the other cosmological parameters are the same as Fig. 6.

by the ASI contract Planck LFI Activity of Phase E2. We thank INFN IS PD51 for partial support. F. F. is partially supported by INFN IS BO 11.

APPENDIX A: ENERGY DENSITY

We use the convolution for the magnetic energy density spectrum in Eq. (16) with the parametrization for the magnetic field PS given in Eq. (17). Since $P_B(k) = 0$ for $k > k_D$, two conditions need to be taken into account:

$$p < k_D, \qquad |\vec{k} - \vec{p}| < k_D. \tag{A1}$$

The second condition introduces a k-dependence on the angular integration domain and the two allow the energy power spectrum to be nonzero only for $0 < k < 2k_D$. Such conditions split the double integral (over γ and over p) in three parts depending on the γ and p lower and upper limit of integration. For simplicity we normalize the Fourier wave number to k_D and we show the integrals with this convention. The splitting in the three parts is shown in

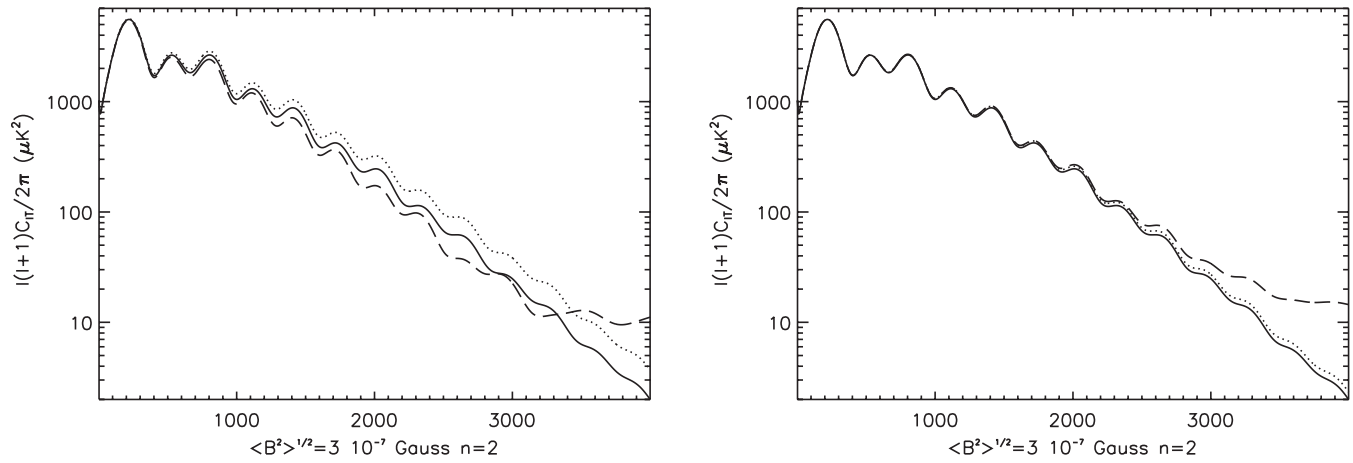

FIG. 12. In the left panel CMB temperature power spectrum obtained with fully correlated PMF with (dashed line) and without (dotted line) Lorentz term in comparison with the vanishing PMF (solid line). As is clear from the previous section, the Lorentz force of a fully correlated magnetic contribution decreases the density contrasts and therefore there is a range in which the CMB TT angular power spectrum is decreased with respect to the adiabatic case. In the right panel we show the same figure with uncorrelated spectra. In the figures $\sqrt{\langle B^2\rangle} = 3 \times 10^{-7}$ Gauss, $k_D = 2\pi$, and $n_B = 2$ are considered. The other cosmological parameters are the same as Fig. 6.

Fig. 14: in region a the angular integration has to be done between -1 and 1, while within b and c regions between $(k^2 + p^2 - 1)/2kp$ and 1.

A sketch of the integration is thus the following:

$$1)\ 0 < k < 1 \int_0^{1-k} dp \int_{-1}^{1} d\gamma \ldots + \int_{1-k}^{1} dp \int_{\frac{k^2+p^2-1}{2kp}}^{1} d\gamma \ldots \equiv \int_0^{1-k} dp I_a(p,k) + \int_{1-k}^{1} dp I_b(p,k)$$

$$2)\ 1 < k < 2 \int_{k-1}^{1} dp \int_{\frac{k^2+p^2-1}{2kp}}^{1} d\gamma \ldots \equiv \int_{k-1}^{1} dp I_c(p,k) \tag{A2}$$

The angular integrals can be performed as

$$I_a = \int_{-1}^{1} p^{n+2}\left[2 - \frac{k^2(1-\gamma^2)}{k^2+p^2-2kp\gamma}\right](k^2 + p^2 - 2kp\gamma)^{n/2} d\gamma = \frac{2p^{n-1}}{kn(2+n)(4+n)}[(k+p)^{n+2}(k^2 - k(2+n)p + (1+4n+n^2)p^2) - |k-p|^{n+2}(k^2 + k(2+n)p + (1+4n+n^2)p^2)], \tag{A3}$$

$$I_b = I_c = \int_{k^2+p^2-1/2kp}^{1} p^{n+2}\left[2 - \frac{k^2(1-\gamma^2)}{k^2+p^2-2kp\gamma}\right](k^2 + p^2 - 2kp\gamma)^{n/2} d\gamma = \frac{p^{n-1}}{4kn(2+n)(4+n)}[8k^4 + 2n - 8k^2 n + 6k^4 n + n^2 - 2k^2 n^2 + k^4 n^2 - 16k^2 p^2 + 24np^2 - 12k^2 np^2 + 6n^2 p^2 - 2k^2 n^2 p^2 + 8p^4 + 6np^4 + n^2 p^4 - 8|k-p|^{n+2}(k^2 + k(2+n)p + (1+4n+n^2)p^2)]. \tag{A4}$$

Note that the divergent terms at the denominator n and $n+2$ simply mean that the above formulae are not applicable for $n = 0$ and $n = -2$ (logarithmic terms appear in these special cases).

Particular care must be used in the radial integrals. In particular, the presence of the term $|k-p|^{n+2}$ in both integrands, needs a further splitting of the integral domain for odd n:

$$\int_0^{(1-k)} dp \to \begin{cases} k < 1/2 \begin{cases} \int_0^k dp \ldots & \text{with} \quad p < k \\ \int_k^{(1-k)} dp \ldots & \text{with} \quad p > k \end{cases} \\ k > 1/2 \quad \int_0^{(1-k)} dp \ldots \quad \text{with} \quad p < k \end{cases}$$

$$\int_{(1-k)}^{1} dp \to \begin{cases} k < 1/2 \quad \int_{(1-k)}^{1} dp \ldots \quad \text{with} \quad p > k \\ k > 1/2 \begin{cases} \int_{(1-k)}^{k} dp \ldots & \text{with} \quad p < k \\ \int_k^1 dp \ldots & \text{with} \quad p > k \end{cases} \end{cases}$$

$$\int_{(k-1)}^{1} dp \to \left\{ 1 < k < 2 \quad \int_{(k-1)}^{1} dp \ldots \quad \text{with} \quad p < k. \right.$$

It is important to study some relevant behavior of the integrands in p. For $p \sim 0$:

$$I_a \sim \tfrac{8}{3} k^n p^{n+2}. \tag{A5}$$

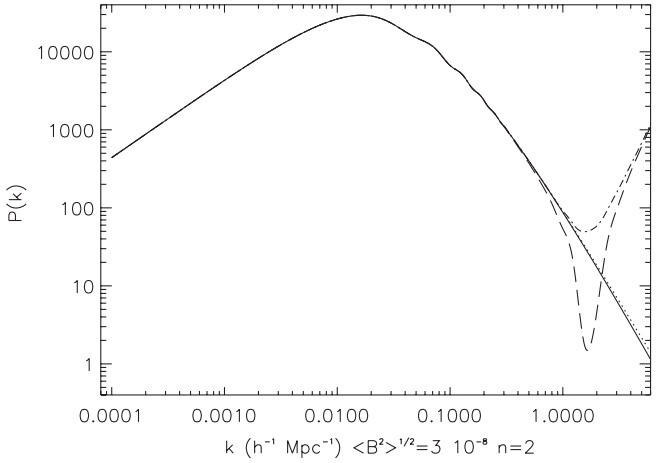

FIG. 13. Linear cold dark matter power spectrum obtained with fully correlated PMF with (dashed line) and without (dotted line) Lorentz term, with uncorrelated PMF, and the Lorentz force (dot-dashed line) in comparison with the vanishing PMF (solid line). In the figure $\sqrt{\langle B^2 \rangle} = 3 \times 10^{-8}$ Gauss, $k_D = 2\pi$, and $n_B = 2$ are considered. The other cosmological parameters are the same as Fig. 6.

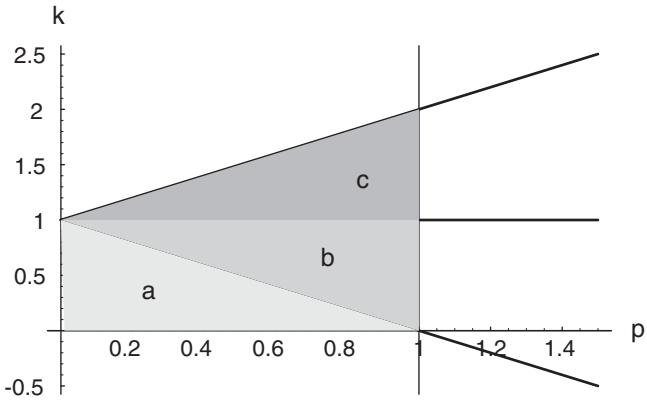

FIG. 14. Integration domains in the (k, p) plane.

For $p \sim k$ the above integrands behave as

$$I_a \sim \frac{2k^{n-2}}{n(n+2)(n+4)}[2^{n+2}k^{n+4}n(n+3) - ((k-p)^2)^{n+2/2}(n+1)(n+4)k^2], \quad \text{(A6)}$$

$$I_b \sim \frac{k^{n-2}}{4n(n+2)(n+4)}[n(4(n+4)k^2+n+2) - 8((k-p)^2)^{n+2/2}(n+1)(n+4)k^2]. \quad \text{(A7)}$$

It is important to stress again that for $n > -3$ the divergences in $p \sim 0$ and $p \sim k$ are integrable.

Following the scheme (A2) we can now perform the integration over p. Our exact results are given for particular values of n_B.

1. $n_B = 4$

$$|\rho_B(k)|^2_{n_B=4} = \frac{A^2 k_D^{11}}{64\pi k_*^8}\left[\frac{4}{11} - \tilde{k} + \frac{4}{3}\tilde{k}^2 - \tilde{k}^3 + \frac{8}{21}\tilde{k}^4 - \frac{\tilde{k}^5}{24} - \frac{\tilde{k}^7}{192} + \frac{\tilde{k}^{11}}{9856}\right]$$

2. $n_B = 3$

$$|\rho_B(k)|^2_{n_B=3} = \frac{A^2 k_D^9}{64\pi k_*^6}\begin{cases} \frac{4}{9} - \tilde{k} + \frac{20}{21}\tilde{k}^2 - \frac{5}{12}\tilde{k}^3 + \frac{4}{75}\tilde{k}^4 + \frac{4}{315}\tilde{k}^6 - \frac{\tilde{k}^9}{525} & \text{for } 0 \le \tilde{k} \le 1 \\ (2-\tilde{k})^2 \frac{264 - 436\tilde{k} + 863\tilde{k}^2 - 528\tilde{k}^3 + 48\tilde{k}^5 + 48\tilde{k}^6 + 16\tilde{k}^7 + 4\tilde{k}^8}{6300k} & \text{for } 1 \le \tilde{k} \le 2 \end{cases}$$

3. $n_B = 2$

$$|\rho_B(k)|^2_{n_B=2} = \frac{A^2 k_D^7}{64\pi k_*^4}\left[\frac{4}{7} - \tilde{k} + \frac{8}{15}\tilde{k}^2 - \frac{\tilde{k}^5}{24} + \frac{11}{2240}\tilde{k}^7\right]$$

4. $n_B = 1$

$$|\rho_B(k)|^2_{n_B=1} = \frac{A^2 k_D^5}{64\pi k_*^2}\begin{cases} \frac{4}{5} - \tilde{k} + \frac{1}{4}\tilde{k}^3 + \frac{4}{15}\tilde{k}^4 - \frac{1}{5}\tilde{k}^5 & \text{for } 0 \le \tilde{k} \le 1 \\ (2-\tilde{k})^2 \frac{8 - 4\tilde{k} - \tilde{k}^2 + 4\tilde{k}^4}{60k} & \text{for } 1 \le \tilde{k} \le 2 \end{cases}$$

5. $n_B = 0$

$$|\rho_B(k)|^2_{n_B=0} = \frac{A^2 k_D^3}{64\pi}\begin{cases} \frac{1}{96\tilde{k}}[\tilde{k}(116 - 102\tilde{k} - 84\tilde{k}^2 + \tilde{k}^3(53 + 4\pi^2) - 24\tilde{k}^3\log[k]^2) \\ \quad + 12\log(1-\tilde{k})(-1 + 4\tilde{k}^2 - 3\tilde{k}^4 + 4\tilde{k}^4\log\tilde{k}) - 48\tilde{k}^4\text{PolyLog}[2, \frac{-1+\tilde{k}}{\tilde{k}}]] & \text{for } 0 \le \tilde{k} \le 1 \\ \frac{1}{96\tilde{k}}[116\tilde{k} - 102\tilde{k}^2 - 84\tilde{k}^3 + 53\tilde{k}^4 + \log[-1+\tilde{k}](-12 + 48\tilde{k}^2 - 36\tilde{k}^4 + 24\tilde{k}^4\log\tilde{k}) \\ \quad + 24\tilde{k}^4\text{PolyLog}[2, \frac{1}{\tilde{k}}] - 24\tilde{k}^4\text{PolyLog}[2, \frac{-1+\tilde{k}}{\tilde{k}}]] & \text{for } 1 \le \tilde{k} \le 2 \end{cases}$$

6. $n_B = -1$

$$|\rho_B(k)|^2_{n_B=-1} = \frac{A^2 k_D k_*^2}{64\pi}\begin{cases} 4 - 5\tilde{k} + \frac{4\tilde{k}^2}{3} + \frac{\tilde{k}^3}{4} & \text{for } 0 \le \tilde{k} \le 1 \\ \frac{((-2+\tilde{k})^2(8 - 4\tilde{k} + 3\tilde{k}^2))}{12\tilde{k}} & \text{for } 1 \le \tilde{k} \le 2 \end{cases}$$

7. $n_B = -3/2$

$$|\rho_B(k)|^2_{n=-3/2} = \frac{A^2 k_*^3}{64\pi}\begin{cases} \frac{1}{45}[\frac{8(-33+29\tilde{k}-4\tilde{k}^2+8\tilde{k}^3)}{\sqrt{1-\tilde{k}}\tilde{k}} + \frac{264}{\tilde{k}} + 60\tilde{k} + 5\tilde{k}^3 - 90\pi \\ +360\log[1+\sqrt{1-\tilde{k}}] - 180\log\tilde{k}] & \text{for } 0 \le \tilde{k} \le 1 \\ \frac{1}{45}[-\frac{8(-33+29\tilde{k}-4\tilde{k}^2+8\tilde{k}^3)}{\sqrt{-1+\tilde{k}}\tilde{k}} + \frac{264}{\tilde{k}} + 60k + 5k^3 - 180\arctan[\frac{1}{\sqrt{-1+\tilde{k}}}] \\ +180\arctan[\sqrt{-1+\tilde{k}}]] & \text{for } 1 \le \tilde{k} \le 2 \end{cases} \quad \text{(A8)}$$

APPENDIX B: LORENTZ FORCE

In order to obtain a complete estimate of the contribution of PMFs to the perturbation, the convolution for the Lorentz force power spectrum is also necessary. The anisotropic stress can be obtained directly from its relation with the Lorentz force and the magnetic energy density. We report here the Lorentz force convolution in Eq. (23) with the magnetic field PS in Eq. (17) for particular values of n_B.

1. $n_B = 4$

$$|L(k)|^2_{n_B=4} = \frac{A^2 k_D^{11}}{64\pi k_*^8}\left[\frac{4}{15} - \frac{2\tilde{k}}{3} + \frac{44\tilde{k}^2}{45} - \frac{5\tilde{k}^3}{6} + \frac{8\tilde{k}^4}{21} - \frac{17\tilde{k}^5}{240} - \frac{\tilde{k}^7}{960} + \frac{\tilde{k}^{11}}{16\,128}\right]$$

2. $n_B = 3$

$$|L(k)|^2_{n_B=3} = \frac{A^2 k_D^9}{64\pi k_*^6}\begin{cases} \frac{44}{135} - \frac{2\tilde{k}}{3} + \frac{556\tilde{k}^2}{735} - \frac{4\tilde{k}^3}{9} + \frac{164\tilde{k}^4}{1575} + \frac{4\tilde{k}^6}{2079} - \frac{11\tilde{k}^9}{11\,025} & \text{for } 0 \le \tilde{k} \le 1 \\ -\frac{44}{135} + \frac{64}{24\,255\tilde{k}^5} - \frac{16}{945\tilde{k}^3} + \frac{88}{525\tilde{k}} + \frac{2\tilde{k}}{3} - \frac{556\tilde{k}^2}{735} + \frac{4\tilde{k}^3}{9} - \frac{164\tilde{k}^4}{1575} - \frac{4\tilde{k}^6}{2079} + \frac{11\tilde{k}^9}{33\,075} & \text{for } 1 \le \tilde{k} \le 2 \end{cases}$$

3. $n_B = 2$

$$|L(k)|^2_{n_B=2} = \frac{A^2 k_D^7}{64\pi k_*^4}\left[\frac{44}{105} - \frac{2\tilde{k}}{3} + \frac{8\tilde{k}^2}{15} - \frac{\tilde{k}^3}{6} - \frac{\tilde{k}^5}{240} + \frac{13\tilde{k}^7}{6720}\right]$$

4. $n_B = 1$

$$|L(k)|^2_{n=1} = \frac{A^2 k_D^5}{64\pi k_*^2}\begin{cases} \frac{44}{75} - \frac{2\tilde{k}}{3} + \frac{32\tilde{k}^2}{105} + \frac{4\tilde{k}^4}{315} - \frac{\tilde{k}^5}{25} & \text{for } 0 \le \tilde{k} \le 1 \\ -\frac{44}{75} + \frac{64}{1575\tilde{k}^5} - \frac{16}{105\tilde{k}^3} + \frac{8}{15\tilde{k}} + \frac{2\tilde{k}}{3} - \frac{32\tilde{k}^2}{105} - \frac{4\tilde{k}^4}{315} + \frac{\tilde{k}^5}{75} & \text{for } 1 \le \tilde{k} \le 2 \end{cases}$$

5. $n_B = 0$

$$|L(k)|^2_{n_B=0} = \frac{A^2 k_D^3}{64\pi}\begin{cases} \frac{43}{48} - \frac{1}{16\tilde{k}^4} - \frac{1}{32\tilde{k}^3} + \frac{7}{48\tilde{k}^2} + \frac{13}{192\tilde{k}} - \frac{67\tilde{k}}{96} + \frac{\tilde{k}^2}{48} + \frac{17\tilde{k}^3}{384} - \frac{\log[1-k]}{16\tilde{k}^5} \\ + \frac{\log[1-k]}{6\tilde{k}^3} - \frac{\log[1-k]}{8\tilde{k}} + \frac{1}{48}\tilde{k}^3\log[1-k] & \text{for } 0 \le \tilde{k} \le 1 \\ \frac{43}{48} - \frac{1}{16\tilde{k}^4} - \frac{1}{32\tilde{k}^3} + \frac{7}{48\tilde{k}^2} + \frac{13}{192\tilde{k}} - \frac{67\tilde{k}}{96} + \frac{\tilde{k}^2}{48} + \frac{17\tilde{k}^3}{384} - \frac{\log[-1+k]}{16\tilde{k}^5} \\ + \frac{\log[-1+k]}{6\tilde{k}^3} - \frac{\log[-1+k]}{8\tilde{k}} + \frac{1}{48}\tilde{k}^3\log[-1+k] & \text{for } 1 \le \tilde{k} \le 2 \end{cases}$$

6. $n_B = -1$

$$|L(k)|^2_{n_B=-1} = \frac{A^2 k_D k_*^2}{64\pi}\begin{cases} \frac{44}{15} - 2\tilde{k} - \frac{4\tilde{k}^2}{105} & \text{for } 0 \le \tilde{k} \le 1 \\ -\frac{44}{15} - \frac{64}{105\tilde{k}^5} + \frac{16}{15\tilde{k}^3} + \frac{8}{3\tilde{k}} + \frac{2\tilde{k}}{3} + \frac{4\tilde{k}^2}{105} & \text{for } 1 \le \tilde{k} \le 2 \end{cases}$$

7. $n_B = -3/2$

$$|L(k)|^2_{n_B=-3/2} = \frac{A^2 k_*^3}{64\pi}\begin{cases} -\frac{1}{8775\sqrt{1-\tilde{k}}\tilde{k}^5}2(-3072 + 3072\sqrt{1-\tilde{k}} + 1536\tilde{k} + 4544\tilde{k}^2 - 4160\sqrt{1-\tilde{k}}\tilde{k}^2 - 1888\tilde{k}^3 \\ +25\,340\tilde{k}^4 - 25\,740\sqrt{1-\tilde{k}}\tilde{k}^4 - 26\,540\tilde{k}^5 - 80\tilde{k}^6 + 160\tilde{k}^7 + 6435\sqrt{1-\tilde{k}}\tilde{k}^5\pi \\ -25\,740\sqrt{1-\tilde{k}}\tilde{k}^5\log[1+\sqrt{1-\tilde{k}}] + 12\,870\sqrt{1-\tilde{k}}\tilde{k}^5\log[\tilde{k}] & \text{for } 0 \le \tilde{k} \le 1 \\ -\frac{1}{8775\sqrt{-1+\tilde{k}}\tilde{k}^5}4(-2(-768(1+\sqrt{-1+\tilde{k}}) + 384\tilde{k} + 16(71 + 65\sqrt{-1+\tilde{k}}\tilde{k}^2 - 472\tilde{k}^3 \\ +(6335 + 6435\sqrt{-1+\tilde{k}})\tilde{k}^4 - 6635\tilde{k}^5 - 20\tilde{k}^6 + 40\tilde{k}^7 + 6435\sqrt{-1+\tilde{k}}\tilde{k}^5\arctan\left[\frac{1}{\sqrt{-1+\tilde{k}}}\right] \\ -6435\sqrt{-1+\tilde{k}}\tilde{k}^5\arctan[\sqrt{-1+\tilde{k}}]) & \text{for } 1 \le \tilde{k} \le 2 \end{cases} \tag{B1}$$

[1] D. Grasso and H. R. Rubinstein, Phys. Rep. **348**, 163 (2001).
[2] M. Giovannini, Classical Quantum Gravity **23**, R1 (2006).
[3] K. Subramanian, arXiv:astro-ph/0601570.
[4] A. Mack, T. Kahniashvili, and A. Kosowsky, Phys. Rev. D **65**, 123004 (2002).
[5] A. Lewis, Phys. Rev. D **70**, 043011 (2004).
[6] R. Durrer, P. G. Ferreira, and T. Kahniashvili, Phys. Rev. D **61**, 043001 (2000).
[7] C. Caprini, R. Durrer, and T. Kahniashvili, Phys. Rev. D **69**, 063006 (2004).
[8] T. Kahniashvili and B. Ratra, Phys. Rev. D **75**, 023002 (2007).
[9] S. Koh and C. H. Lee, Phys. Rev. D **62**, 083509 (2000).
[10] D. G. Yamazaki, K. Ichiki, T. Kajino, and G. J. Mathews, Astrophys. J. **646**, 719 (2006).
[11] M. Giovannini and K. E. Kunze, Phys. Rev. D **77**, 063003 (2008).
[12] A. Lewis, A. Challinor, and A. Lasenby, Astrophys. J. **538**, 473 (2000).
[13] J. A. Adams, U. H. Danielsson, D. Grasso, and H. Rubinstein, Phys. Lett. B **388**, 253 (1996).
[14] C. P. Ma and E. Bertschinger, Astrophys. J. **455**, 7 (1995).
[15] M. Giovannini, Phys. Rev. D **74**, 063002 (2006).
[16] D. Paoletti, Einstein-Boltzmann Codes for Cosmic Microwave Background Anisotropies with Primordial Magnetic Fields, Tesi di Laurea Specialistica in Astrofisica e Cosmologia, March 2007, Universitá degli Studi di Bologna (unpublished).
[17] M. Abramowitz and I. Stegun, *Handbook of Mathematical Functions with Formulas, Graphs, and Mathematical Table* (Dover Publishing, New York, 1965).
[18] I. Brown and R. Crittenden, Phys. Rev. D **72**, 063002 (2005).
[19] D. G. Yamazaki, K. Ichiki, T. Kajino, and G. J. Mathews, Phys. Rev. D **77**, 043005 (2008).
[20] A. Kosowsky, T. Kahniashvili, G. Lavrelashvili, and B. Ratra, Phys. Rev. D **71**, 043006 (2005).
[21] Planck Collaboration, arXiv:astro-ph/0604069.
[22] D. G. Yamazaki, K. Ichiki, and T. Kajino, Astrophys. J. **625**, L1 (2005).